Current Biology, Vol. 14, 88–98, January 20, 2004, ©2004 Elsevier Science Ltd. All rights reserved. DOI 10.1016/j.cub.2004.01.003

Protein Kinase D-Mediated Anterograde Membrane Trafficking Is Required for Fibroblast Motility

Natalie L. Prigozhina
and Clare M. Waterman-Storer*
The Scripps Research Institute
10550 N. Torrey Pines Road
Department Cell Biology, CB163
La Jolla, California 92037

Summary

Background: Locomoting cells exhibit a constant retrograde flow of plasma membrane (PM) proteins from the leading edge lamellipodium backward, which when coupled to substrate adhesion, may drive forward cell movement. However, the intracellular source of these PM components and whether their continuous retrograde flow is required for cell motility is unknown.
Results: To test the hypothesis that the anterograde secretion pathway supplies PM components for retrograde flow that are required for lamellipodial activity and cell motility, we specifically inhibited transport of cargo from the trans-Golgi network (TGN) to the PM in Swiss 3T3 fibroblasts and monitored cell motility using time-lapse microscopy. TGN-to-PM trafficking was inhibited with a dominant-negative, kinase-dead (kd) mutant of protein kinase D1 (PKD) that specifically blocks budding of secretory vesicles from the TGN and does not affect other transport pathways. Inhibition of PKD on the TGN inhibited directed cell motility and retrograde flow of surface markers and filamentous actin, while inhibition of PKD elsewhere in the cell neither blocked anterograde membrane transport nor cell motile functions. Exogenous activation of Rac1 in PKD-kd-expressing cells restored lamellipodial dynamics independent of membrane traffic. However, lamellipodial activity was delocalized from a single leading edge, and directed cell motility was not fully recovered.
Conclusions: These results indicate that PKD-mediated anterograde membrane traffic from the TGN to the PM is required for fibroblast locomotion and localized Rac1-dependent leading edge activity. We suggest that polarized secretion transmits cargo that directs localized signaling for persistent leading edge activity necessary for directional migration.

Introduction

The ability to locomote directionally and persistently is a property of many cell types and is essential for development, wound healing, the immune response, and tissue remodeling. Locomotion of vertebrate tissue cells in culture depends on the protrusion of a flat, thin lamellipodium in the direction of migration at the leading edge of the cell. If a protruding lamellipodium attaches to the substrate, it provides an anchor for forces pulling the cell body forward. If it fails to attach to the substrate, it bends back toward the cell body and becomes a membrane ruffle, which moves on the dorsal cell surface toward the cell center in a process called retrograde flow [1–3]. In addition to membrane ruffles, particles adhering to either the dorsal or ventral cell surfaces undergo retrograde flow from the leading edge [4–6]. When coupled to substrate adhesion, the forces generated to drive retrograde flow are thought to mediate cell motility.

The nature of this retrograde flow has been the subject of much controversy (reviewed by [2]). The lipid flow hypothesis [7] proposed that the driving force for retrograde flow was supplied by directed insertion of membrane lipids from an intracellular store into the leading edge plasma membrane (PM) by exocytosis and their subsequent removal from sites distal from the leading edge by endocytosis. However, by monitoring the movement of specifically marked PM molecules, it was shown that only PM proteins flow rearward, while lipids do not [8–10]. Subsequently it was shown that actin polymerizes just subadjacent to the PM along the leading edge and then undergoes retrograde flow at a similar rate as PM protein-coupled markers [3, 4, 11, 12]. Thus, it is now generally accepted that moving filamentous actin is responsible for generating the forces both for the initial lamellipodial protrusion [1, 3] and for the retrograde flow of ruffles, PM proteins, and PM bound markers [1, 3, 9]. Although actin dynamics are responsible for retrograde flow, it is still unknown whether a constant supply of PM components is needed at the leading edge for directed motility, and their intracellular source remains obscure.

One hypothesis is that the anterograde membrane transport pathway, which transmits cargo from the endoplasmic reticulum (ER) through the Golgi apparatus (GA) and trans-Golgi network (TGN) to be secreted at the PM, may be the intracellular source for PM components at the leading edge to supply retrograde flow. In support of this, when cells undergo directed migration, the GA is oriented between the nucleus and leading edge [13, 14], where secretory vesicle cargo becomes preferentially localized [15, 16]. Treatment with brefeldin A, a pleiotropic agent whose best characterized effect on cells is disruption of anterograde membrane transport, inhibits fibroblast motility [17]. Despite this indirect evidence, specific blockage of late stages of the secretory pathway to test its role in cell motility has not been performed.

Here, we provide the first direct testing of the hypothesis that in fibroblasts, the anterograde secretion pathway is required for directed cell motility. To block a late stage in this transport pathway we use a dominant-negative mutant (kinase-dead [kd]) of protein kinase D1 (PKD), in which Lys^{618} is changed to Asn (K618N) [18, 19] to inhibit TGN-to-PM transport. PKD is localized primarily to the TGN by virtue of a cysteine-rich C1a domain that binds to diacylglycerol (DAG), and mutation in Pro^{155} (P155G) abrogates its association with the TGN [20–23]. In some cell types, PKD may also either remain

*Correspondence: waterman@scripps.edu

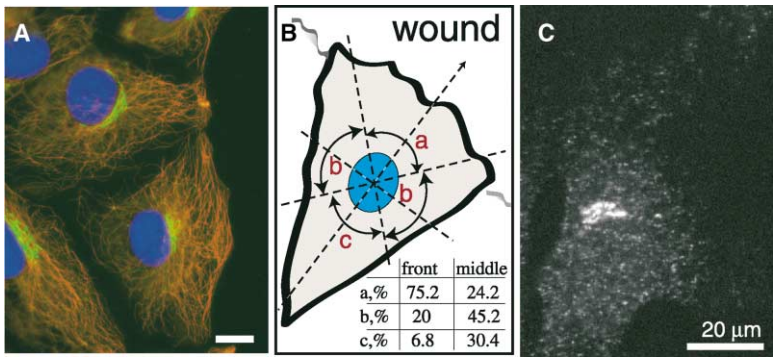

Figure 1. The GA in Migrating Swiss 3T3 Fibroblasts Is Oriented toward the Direction of Migration

(A) Fibroblasts fixed 4 hr after initiation of migration in a wound-healing assay; nuclei, blue; microtubules, red; and mannosidase-II-labeled medial GA, green.

(B) Cartoon illustrating criteria used for scoring the position of the GA (in % of all cells, N=500) relative to the nucleus: a, forward; b, lateral; and c, rear. Front, first row of cells migrating into the wound; middle, five cell rows inland from the wound edge.

(C) Compact TGN in a control 3T3 cell visualized using antibodies against TGN38. Scale bars 20 μm.

soluble or associate with the PM by virtue of its C1b domain where Pro^{287} is crucial for PM binding [24–26]. PKD activity on the TGN is required for budding of PM-destined secretory vesicles from the TGN while having no effect on other transport steps [19]. PKD's TGN-associated substrate is unknown, although possible candidates include lipid kinases that generate fission-promoting lipids [19, 27]. Nevertheless, PKD-kd is a useful tool for manipulating TGN to PM transport. Indeed, we find that inhibition of PKD function on TGN membranes specifically blocks anterograde transport from the TGN to PM, while inhibition of PKD elsewhere in the cell does not. Specific blockage of PKD-mediated TGN to PM transport also inhibits leading edge lamellipodial activity, retrograde flow, and cell motility. Exogenous activation of the small GTPase regulator of lamellipodial activity, Rac1, in cells expressing PKD-kd recovers lamellipodial activity independent of anterograde membrane trafficking. Thus, we suggest that PKD-mediated polarized membrane transport may direct localized signaling required for leading edge lamellipodial dynamics that mediate directed cell motility.

Results

Inhibition of PKD at the TGN in Swiss 3T3 Cells Inhibits Anterograde Membrane Transport

Swiss 3T3 fibroblasts were chosen as a model system for studying the role of anterograde membrane trafficking in cell motility. As in other cell types [13, 14], in Swiss 3T3 fibroblasts the Golgi apparatus (Figures 1A and 1B) and TGN (Figure 1C) orient in the direction of cell migration both in a monolayer wound assay and in randomly migrating individual cells.

To test the role of anterograde membrane trafficking in Swiss 3T3 cell migration, we sought to specifically inhibit TGN to PM transport. Previous studies in HeLa cells demonstrated that expression of a dominant-negative, kinase-dead mutant of PKD1 (PKD-kd) causes tubulation of TGN membranes and arrest of PM-destined membrane transport [19]. In control 3T3 fibroblasts, both the GA (Figure 1A) and the TGN (Figure 1C) appear as compact perinuclear organelles. When green fluorescent protein (GFP)-fused PKD-kd (PKD-kd-GFP) was expressed in these cells, it localized to long tubules that emanated from central cell regions (Figure 2A) and colocalized with the TGN resident protein TGN38 (Figures 2C–2E). We analyzed the behavior of the PKD-kd-GFP-labeled tubules by time-lapse spinning-disk confocal microscopy and found that they were highly dynamic, they extended and retracted from the TGN (but hardly ever detached), and they did not fuse with the PM (Figures 2A and 2B, Supplemental Movie 1).

To confirm that anterograde membrane transport was inhibited by PKD-kd expression, we coexpressed a GST-fused PKD-kd together with a well-characterized marker for the anterograde secretion pathway, the temperature-sensitive ts042 mutant of vesicular stomatitus virus glycoprotein (VSVG) conjugated with GFP [28]. To quantify the efficiency of VSVG-GFP transport from the ER to the GA to the PM, we measured its fluorescence intensity in peripheral regions of the cell relative to the total fluorescence intensity of the whole cell. This analysis confirmed that in control 3T3 cells, VSVG-GFP was indeed retained from transport in the peripheral ER at the restrictive temperature (Figures 3C and 3E). Upon shift to the permissive temperature (37°C), it was rapidly transported by tubulovesicular carriers to the centrally located perinuclear GA (Supplemental Movie 2), corresponding to a drop in peripheral fluorescence (Figures 3C and 3F). VSVG-GFP exit from the TGN was marked by an increase in peripheral fluorescence (Figures 3C, 3D, 3G) as transport vesicles fused with the PM, often near protruding lamellipodia (Figures 3A and 3B, Supplemental Movie 2).

In contrast, VSVG-GFP trafficking in cells expressing PKD-kd was inhibited. Although VSVG-GFP moved to the GA with normal kinetics after shift to 37°C (Figures 3C, 3H, and 3I), the exit of VSVG-GFP from the TGN was impaired. Instead, VSVG-GFP remained in membrane tubules that emanated from the TGN (Supplement Movie 3) and seldom detached. VSVG-GFP fluorescence in the peripheral PM did not increase with time, indicating that VSVG-GFP was not being delivered to the PM (Figures 3C, 3D, 3I, and 3J). The average peripheral fluorescence measured after 40 or more minutes at 37°C was only 40.5% ± 6.1% ($n = 5$) of the total fluorescence compared to 79.4% ± 10.4% ($n = 5$) in control cells (Figure 3D). In contrast, expression of PKD-kd mutants that are defective in binding both the TGN and the PM (PKD-kd-P155/287G) or TGN alone (PKD-kd-P155G) and which instead localize diffusely in the cytoplasm in Swiss 3T3

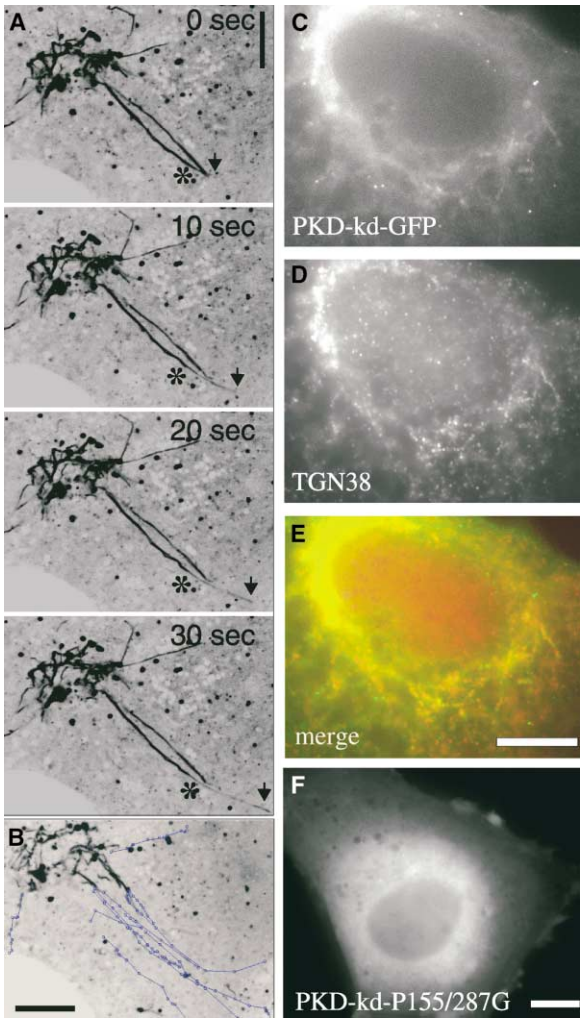

Figure 2. PKD-kd-GFP Localizes to Dynamic TGN-Derived Tubules in 3T3 Fibroblasts

(A and B) PKD-kd-GFP dynamics in a living cell, contrast inverted. (A) Confocal images from a time-lapse series (10 s intervals) showing long membrane tubules labeled with PKD-kd-GFP. Arrow, end of a dynamic membrane tubule. Asterisk, end of a second membrane tubule extending along the same track. (B) First image from the time-lapse used in (A) showing tracks of the tips of the growing PKD-kd-GFP labeled membrane tubules over 20 min.

(C–E) PKD-kd-GFP colocalizes with the TGN in fixed cells. (C) Tubulated TGN labeled by PKD-kd-GFP (green) and (D) anti-TGN38 immunofluorescence (red). (E) Composite image of (C) and (D) showing colocalization (yellow).

(F) Cell expressing nonmembrane-targeted PKD-kd-P155/287G conjugated with GFP, showing cytoplasmic localization. Scale bars = 10 μm.

fibroblasts (Figure 2F and data not shown) did not affect VSVG-GFP trafficking (Figures 3C and 3D). We also found that the tips of the growing PKD-kd-GFP-labeled tubules (Figure 2B) translocated with the same rates as VSVG-GFP-labeled anterograde transport carriers in control cells (mean average velocities of 0.292 ± 0.001 μm/s and 0.290 ± 0.007 μm/s, respectively), suggesting a common mechanism.

To examine the transport process further and, in particular, determine if the lack of VSVG-GFP in the PM in PKD-kd-expressing cells was due to an increase in PM reinternalization by endocytosis, we pulse-labeled VSVG on the cell surface with antibodies against the extracellular domain of VSVG. Cells were incubated for 75 min after the shift to permissive temperature, with the last 30 min of incubation being in the presence of antibodies. The cells were then fixed and analyzed for the VSVG localization both by GFP fluorescence and spectrally distinct immunofluorescense. We found that in control cells, but not in PKD-kd-expressing cells, VSVG-GFP strongly colocalized with the antibody signal at the PM (Figures 3K and 3L). Relative fluorescence intensity of the antibody labeling on the surface of the cells normalized to the total amount of cellular VSVG-GFP fluorescence was 4.2 times greater in control cells compared to PKD-kd-expressing cells, confirming inhibition of anterograde transport found with the live cell analysis (Figure 3D). Furthermore, GA and other intracellular structures within both control and PKD-kd-expressing cells were nearly all labeled exclusively with VSVG-GFP and not with the antibody, indicating that they had not been reinternalized after secretion. Together, these results demonstrate that inhibition of PKD function specifically at the TGN inhibits the anterograde membrane trafficking pathway of Swiss 3T3 cells.

Inhibition of Anterograde Trafficking Blocks Lamellipodial Activity and Cell Motility

To determine the effects of blocking anterograde transport on cell motility, we allowed 3T3 cells to express PKD-kd-GFP for at least 4 hr and then used time-lapse phase-contrast microscopy to analyze cell migration. During a 2 hr observation time, control cells changed their shape extensively, exhibited lamellipodial protrusion/retraction and ruffling activity, and migrated a considerable distance (Figure 4A). In stark contrast, cells in which the transport from the TGN to the PM was blocked by PKD-kd-GFP expression had nearly quiescent edges and barely changed shape during the 2 hr of observation (Figure 4B, Supplemental Movie 4). Indeed, tracking of nuclear positions at 4 min intervals in control and PKD-kd-expressing cells (Figure 4C) revealed that the mean average instantaneous migration rate of the PKD-kd-expressing cells (0.15 ± 0.01 μm/min; median 0.12 μm/min) was significantly lower than that of the control cells (0.29 ± 0.01 μm/min; median 0.25 μm/min), cells expressing GFP alone (0.27 ± 0.01 μm/min; median 0.21 μm/min), cells expressing nonmembrane-targeted PKD-kd-P155/287G (0.28 ± 0.01 μm/min; median 0.25 μm/min), or cells expressing the non-TGN-targeted PKD-kd-P155G (0.29 ± 0.01 μm/min; median 0.26 μm/min). In support of this data, we used another, unrelated way to inhibit anterograde transport pathway by disrupting ARF1 function. ARF1 is a well characterized small GTPase that regulates transport between ER and GA, and expression of the dominant-negative GDP bound mutant ARF1-T31N inhibits anterograde membrane trafficking from the ER to the GA [29]. Similar to PKD inhibition, we found that motility of Swiss 3T3 fibroblasts microinjected with ARF1-T31N protein was greatly reduced (mean average velocity 0.14 μm/min) compared to control noninjected cells (Figure 4C) and cells injected with buffer alone (data not shown).

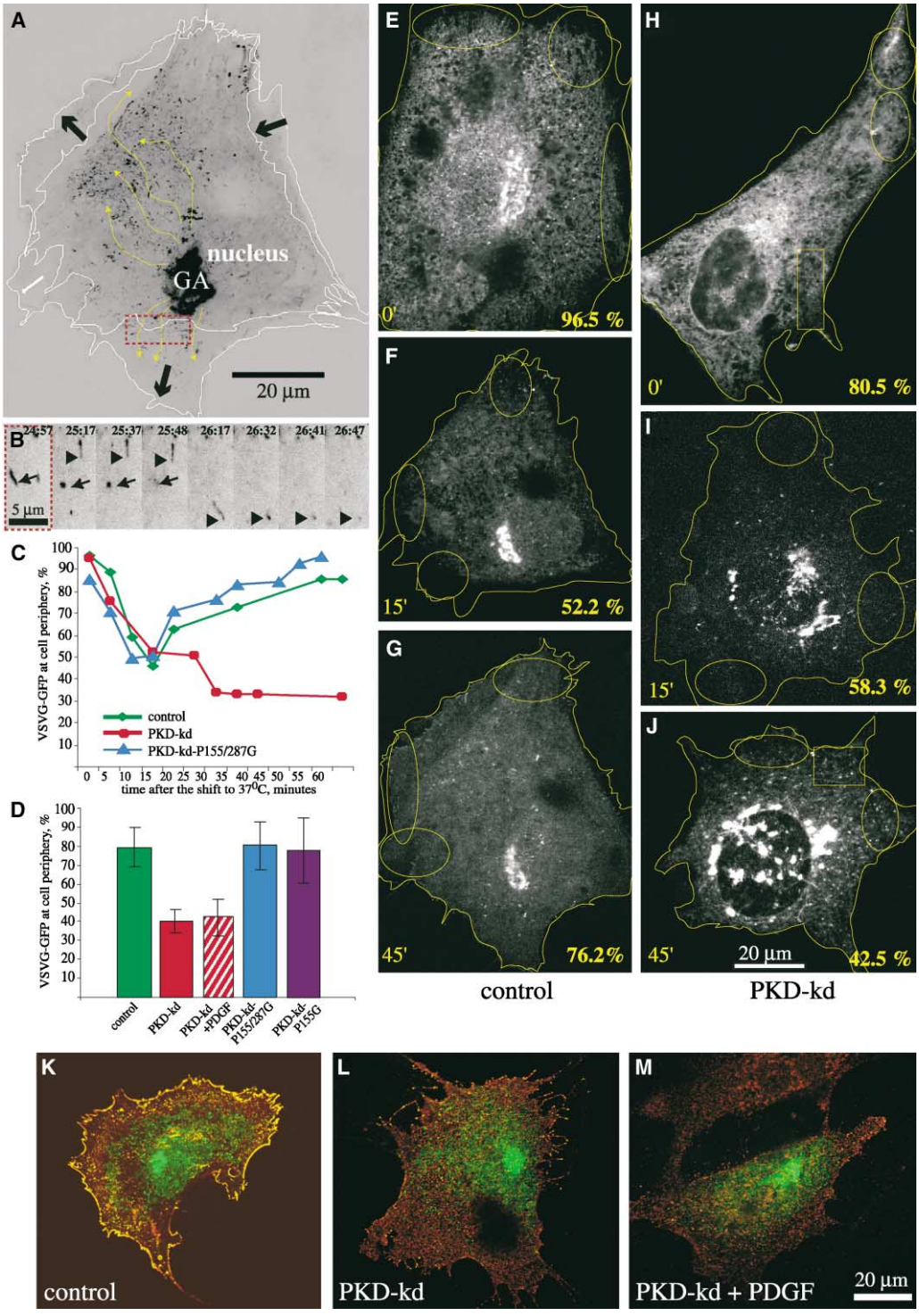

Figure 3. Transport of VSVG-GFP Is Inhibited in PKD-kd-Expressing Cells

(A) Control cell. VSVG-GFP-labeled transport carriers are primarily transported toward the protruding cell edges. The image is a maximal projection from time-lapse series. Cell contours are outlined twice: when export from the Golgi area began (15 min after shift to the permissive temperature) and at the end of the experiment, 30 min later. Thick, black arrows indicate the direction of cell edge motion. Tracks of VSVG-GFP carriers leaving the GA and going toward protruding cell edges are highlighted with thin, yellow arrows. Contrast inverted.

(B) Examples (arrows and arrowheads) of VSVG-GFP carriers fusing with the PM at the cell periphery in the area indicated by red-dashed line in (A). Note the spreading of the GFP label concurrent with the vesicle disappearance, indicating fusion with the PM. Time (min:sec) at the permissive temperature is indicated.

(C) Dynamics of VSVG-GFP trafficking in control cells and cells expressing PKD-kd or PKD-kd-P155/287G (data from single representative experiments). Relative fluorescence intensity of the VSVG-GFP signal at the cell periphery relative to total fluorescence intensity of the whole

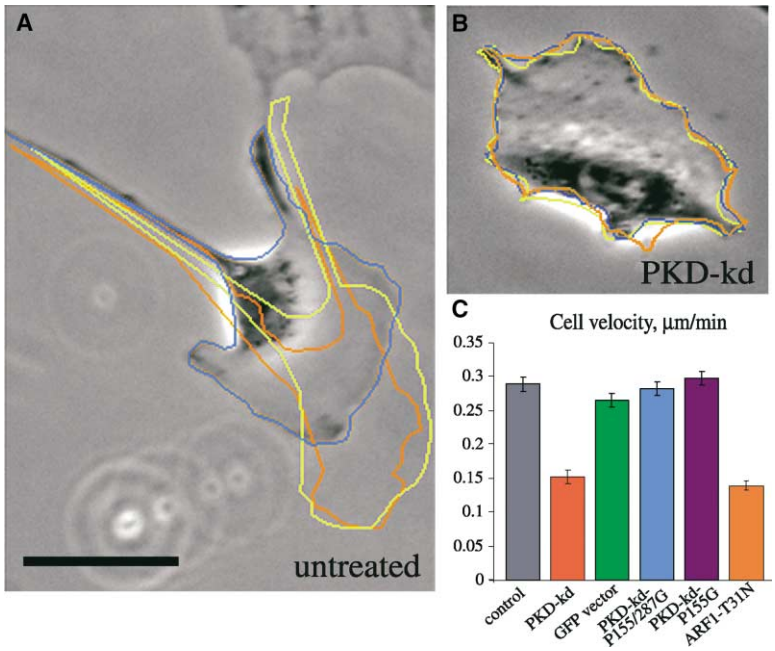

Figure 4. Blockage of the Anterograde Secretion Pathway Inhibits Cell Motility

(A) Control and (B) PKD-kd-injected Swiss 3T3 cells, outlined every hour during a time-lapse series (blue, time 0; yellow, 1 hr; and orange, 2 hr); first image of the series is shown. The control cell (A) is highly polarized and exhibits net migration, while the PKD-kd-expressing cell (B) shows no migration and very little shape change. Scale bar 50 μm; (A) and (B) are at the same magnification.

(C) Mean average velocities (± standard errors of the mean) of control noninjected cells (18 cells), cells expressing GFP (6 cells), PKD-kd-GFP (14 cells), PKD-kd-P155/287G-GFP (9 cells), PKD-kd-P155G-GFP (18 cells), and cells microinjected with ARF1-T31N (24 cells) were calculated from at least three different experiments. N(control) = 335; N(GFP) = 419; N(PKD-kd) = 222; N(PKD-kd-P155/287G) = 257, N(ARF-T31N) = 259, where N equals the number of 20 min intervals used to determine average velocities (see Experimental Procedures).

To assess directional persistence of migration, we compared how far the control and experimentally perturbed cells moved from their origin in 20 min intervals. Control cells migrated significantly longer distances compared to the cells expressing PKD-kd-GFP (median 3.2 μm and 0.97 μm, respectively; Figure 6H), while expression of the nonmembrane-targeted PKD-kd-P155/287G or GFP alone did not significantly affect the persistence of migration (median 2.9 μm and 3.0 μm, respectively). Together, these results demonstrate that cell motility is impaired when anterograde membrane transport from the TGN to the PM is specifically inhibited.

Inhibition of Anterograde Trafficking by PKD-kd Inhibits Retrograde Flow

To determine if inhibition of anterograde membrane transport affected retrograde flow of cell surface bound markers, we tracked the motion of aminated polystyrene beads coupled to the cell surface that were within 20 μm from nonretracting cell edges (Figures 5A and 5B). In control cells, 80.5% of beads moved toward the cell center on well-oriented centripetal trajectories (Figure 5A). In contrast, no more than 25% of the beads on the cells expressing PKD-kd-GFP moved in the retrograde direction (i.e., nonparallel to the cell edge, Figure 5B). The few beads that did move on cells expressing PKD-kd moved with approximately the same velocity as beads moving on control cells (median values 0.43 μm/min for control and 0.44 μm/min for PKD-kd-GFP), but they generally had less-oriented trajectories than on control cells (e.g., beads 2–4 in Figure 5B). Thus, inhibition of the anterograde secretory pathway with PKD-kd perturbs the rearward movement of surface-coupled beads.

One possibility for why PKD-kd expression affected retrograde flow and cell motility is that it perturbed cytoskeletal organization. To address this question, we fixed PKD-kd-GFP-expressing cells and immunolocalized microtubules and stained polymerized actin with rhodamine-phalloidin. This revealed no effect of PKD-

cell is plotted against time after shift to the permissive temperature to initiate VSVG-GFP transport through the secretory pathway. At the beginning of the experiment, VSVG-GFP is arrested in the ER, corresponding to high peripheral fluorescence. By 15 min, it is transported to the central GA/TGN, causing a decrease in peripheral fluorescence. Finally, as VSVG-GFP leaves the GA/TGN area and moves to the PM (in control cells), peripheral fluorescence rises again. In contrast, in PKD-kd-expressing cells, VSVG-GFP never leaves the central area (TGN) of the cell, so the peripheral fluorescence remains low.

(D) The average fluorescence intensity of VSVG-GFP at the cell periphery at least 40 min after the shift to permissive temperature (control cells; cells expressing PKD-kd, PKD-kd-P155/287G or PKD-kd-P155G; cells expressing PKD-kd and treated with PDGF for at least 15 min) is shown. Representative images of VSVG-GFP expressing control cells (E–G) and cells coexpressing GST-tagged PKD-kd (H–J), illustrating VSVG-GFP localization at various times after the shift to permissive temperature (shown in minutes in the lower left). Relative peripheral fluorescence (in percentage of total fluorescence intensity) of VSVG-GFP for each image is indicated in the lower right. The regions of the cells used for fluorescence intensity measurements are outlined (see Experimental Procedures).

(K–M) Pseudocolored images showing VSVG-GFP signal (green) and antibodies against extracellular domain of VSVG (red) in a control cell (K), a cell expressing PKD-kd (L), and a cell expressing PKD-kd and additionally treated with PDGF (M). Yellow indicates colocalization, primarily in the PM of the control cell (K). Note that the PKD-kd-expressing cells exhibit background levels of immunofluorescence, comparable to that of a noninjected cell in (M). (E)–(J) and (K)–(M) are shown at the same magnification.

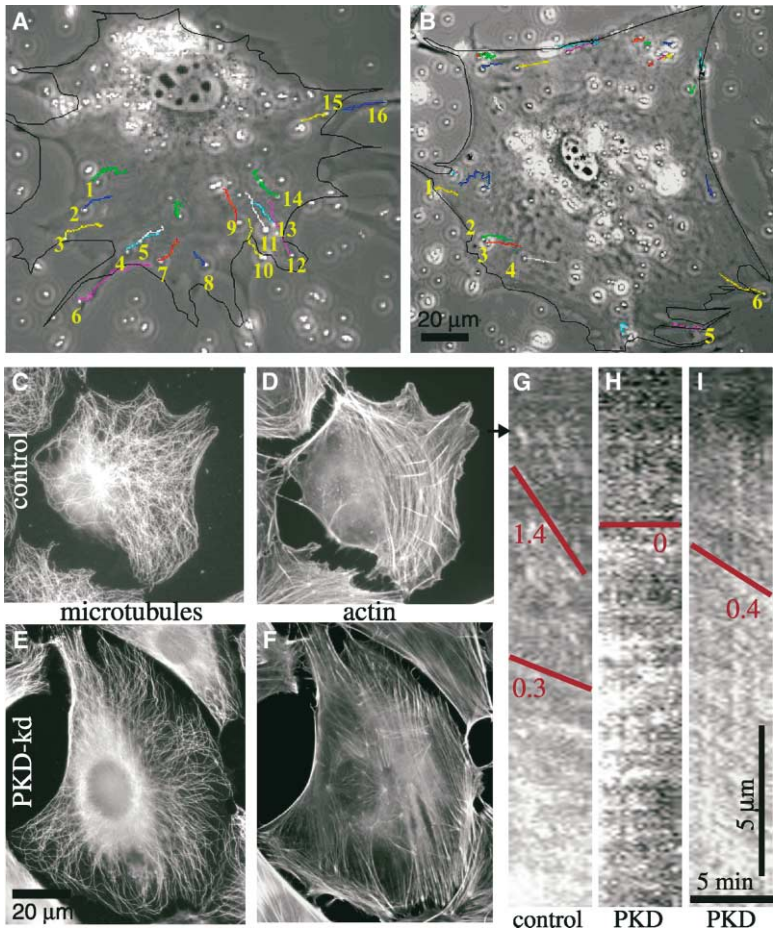

Figure 5. PKD-kd Expression Inhibits Retrograde Flow of Surface-Coupled Aminated Beads and Lamellum Actin

Tracks of aminated beads (colored lines) on the surface of a control (A) and a PKD-kd-expressing cell (B). Each image shows the cell in the initial position at the beginning of the time lapse and the outline of the same cell at the end of the time lapse (50 min later). Beads that were considered to be moving retrograde are numbered. The number is placed near the original position of the bead. Cytoskeleton in control (C and D) and PKD-kd-GFP-expressing (E and F) cells. (C and E) MTs visualized with antibodies against tubulin. (D and F) Actin cytoskeleton visualized by rhodamine-phalloidin staining. Actin in the control cell (D) reveals actin-rich lamellipodia, while inhibition of PKD reduces lamellipodia (F). (G–I) Kymographs showing actin retrograde flow made from 5 min time-lapse movies of cells injected with low levels of rhodamine-labeled actin. Location of the cell edge is indicated by the arrow. Red lines are used to highlight the slopes representing the rate of actin retrograde flow over time (shown next to each line). (G) Control cell exhibiting rapid retrograde flow in the lamellipodium and slower flow in the lamellum. (H) Typical edge of a PKD-kd-GFP-expressing cell with no actin flow. (I) Slow retrograde flow corresponding to a rare instance of edge activity on a PKD-kd-expressing cell. Scale bars for (A)–(F) are 20 μm.

kd-GFP on the organization of microtubules as compared to controls (Figures 5C and 5E). However, PKD-kd-expressing cells often lacked narrow lamellipodial actin meshworks at their noncontacted edges (Figure 5F) that were typical of actively migrating control cells (Figure 5D). This suggested that inhibition of anterograde membrane transport may have an effect on actin cytoskeleton dynamics.

To determine if the inhibition of retrograde bead movement on lamellipodia of PKD-kd-GFP-expressing cells was due to changes in the dynamics of the underlying actin, we employed time-lapse confocal fluorescent speckle microscopy [12, 30]. In this technique, low levels of fluorescent actin are injected into cells, creating fluorescent speckles in the lamellipodium and lamellum actin meshwork that serve as fiduciary marks, allowing direct measurement of actin retrograde flow velocity by kymograph analysis of time-lapse image series [12].

As has been observed in other cell types [30, 31], in control 3T3 fibroblasts actin underwent rapid retrograde flow at 1.4 ± 0.5 μm/min in the lamellipodium within 5 μm from the leading edge and slowed down to 0.3 ± 0.1 μm/min in the lamellum at ~5 to ~10 μm from the leading edge (Figure 5G). In contrast, in PKD-kd-GFP-expressing cells there was very little or no retrograde flow of actin (Figure 5H), although when present, actin flow was 0.4 ± 0.2 μm/min (Figure 5I), with the region of fast lamellipodial flow absent. Together, these results show that inhibition of anterograde membrane transport by PKD-kd suppresses retrograde flow of actin and cell surface bound markers.

Lamellipodial Activity Can Be Induced in PKD-kd-Expressing Cells by Exogenous Rac1 Activation

Since PKD-mediated anterograde membrane transport was required for actin-dependent ruffling and retrograde flow at the leading edge to promote directed cell motility, we sought to determine if this pathway was delivering a signal required for localized actin dynamics. One obvious candidate is Rac1, a small GTPase signaling protein, which via downstream effectors activates actin polymerization and lamellipodia formation in Swiss 3T3 cells [32, 33]. To determine if exogenous Rac1 activation could overcome the PKD-kd-induced inhibition of motile activities, we coexpressed PKD-kd-GFP and Rac1-Q61L, a constitutively active mutant of Rac1 or, alternatively, we treated PKD-kd-GFP-expressing cells with platelet-derived growth factor (PDGF), which is an upstream activator of Rac1 [32, 33]. Cells expressing Rac1-Q61L and cells treated with PDGF were virtually indistinguishable from each other whether or not they were, in addition, expressing PKD-kd-GFP to inhibit anterograde membrane transport. In all four cases, cells exhibited a flattened and spread morphology and lamellipodial protrusion/retraction activity throughout the cell periph-

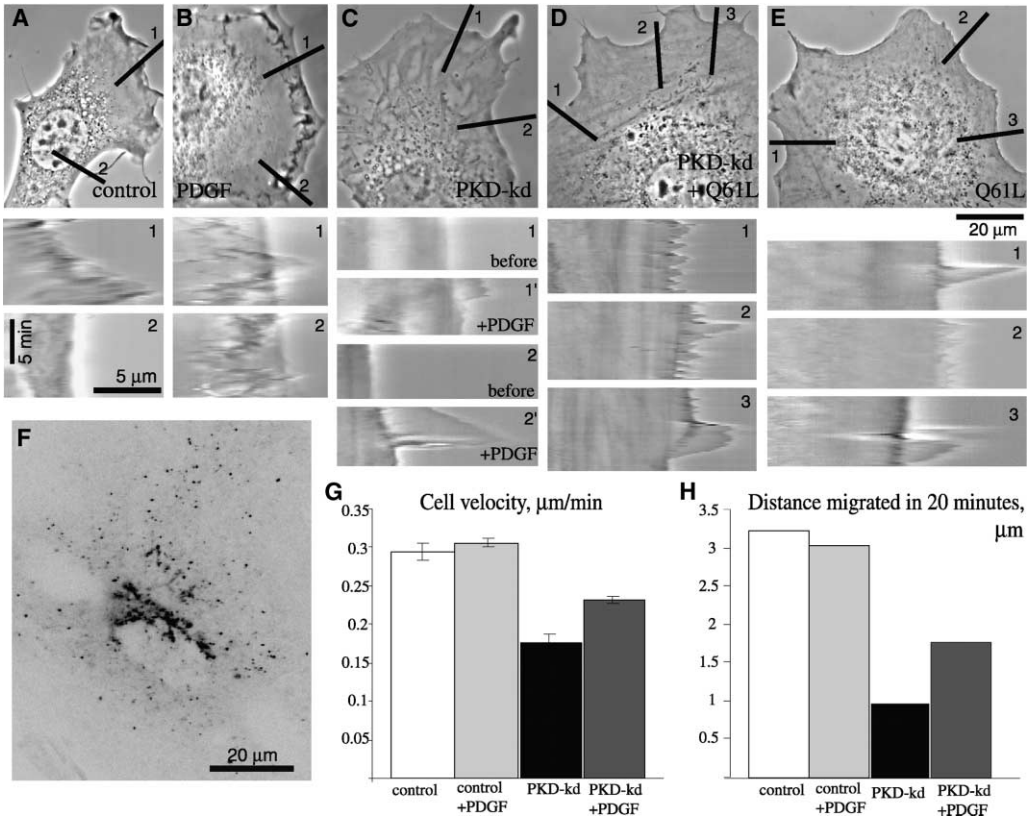

Figure 6. Inhibition of Ruffling Activity in PKD-kd-Expressing Cells Can Be Rescued by Addition of PDGF or Expression of Dominant-Active Rac1

(A–E) Cells were filmed by time-lapse phase-contrast microscopy. Top: first images from the image series are shown for control cell (A), PDGF-treated cell (B), PKD-kd-GFP-expressing cell (C), cell expressing both PKD-kd-GFP and Rac1-Q61L (D), and Rac1-Q61L expressing cell (E). Bottom: kymographs of the protrusive activity of the cell edges taken along the lines highlighted in the top panels. When the cell edge is actively moving, this is seen in the kymographs as variable positions along the x axis over time (y axis). Control untreated cell (A) exhibits polarized lamellipodial activity at the leading edge (kymograph 1) and no activity along other edges (kymograph 2). For the PKD-kd-expressing cell in (C), kymographs show cell edge motion before (1 and 2) and after (1′ and 2′) PDGF addition. Note the flat "edge" in kymographs means no lamellipodial activity in PKD-kd-expressing cells. Compare it with high variability in kymographs (1′ and 2′) taken after addition of PDGF and indicating increased protrusional activity of the cell edge.

(F) VSVG-GFP-labeled GA/TGN in a PKD-kd-expressing cell treated with PDGF. Contrast inverted.

(G) Mean average velocities of migration of control untreated cells, control cells treated with PDGF, PKD-kd-expressing cells, and PKD-kd expressing cells treated with PDGF (± standard errors of the mean). N(control) = 263; N(Control + PDGF) = 993; N(PKD-kd) = 236; N(PKD-kd + PDGF) = 676, where N equals the number of 20 min intervals used to determine average velocities.

(H) Median distances (in μm) that cells travel from their origins over a 20 min interval. The data are calculated from a time-lapse series with 20 min intervals between frames. Scale bar for cell images is 20 μm; all cell images are shown at the same magnification. For kymographs (all shown at the same scale), scale bar is 5 μm and time scale is 5 min.

ery (Figures 6B–6E). This was in contrast to untreated control cells, where lamellipodial activity was confined primarily to a single leading edge (Figure 6A), with non-leading cell edges remaining quiescent. In addition, within 3 min of application, PDGF induced appearance of large dorsal ruffles (seen as dark smears in kymographs) and edge protrusions in both control and PKD-kd-GFP-expressing cells (Figures 6B and 6C).

Since PDGF and Rac1-Q61L produced similar phenotypes in PKD-kd-expressing cells, we used PDGF treatment for further study. First, we found that although PDGF increased lamellipodial activity in PKD-kd-expressing cells, it did not fully restore their ability to migrate (Figures 6G and H). Then, to verify that PDGF did not restore membrane transport in PKD-kd-expressing cells, we examined VSVG-GFP trafficking. Although the TGNs in these cells appeared vesiculated (Figure 6F), the vesicles rarely moved and did not fuse with the PM (data not shown). The inhibition of anterograde trafficking in PKD-kd-expressing cells treated with PDGF was confirmed by our fluorescence microscopy analysis of VSVG-GFP transport from the peripheral ER to the cell center and back to the peripheral plasma membrane (at least 45 min after induction of VSVG-GFP transport by temperature shift followed by at least 15 min of PDGF treatment, Figure 3D). This analysis showed that relative VSVG-GFP fluorescence at the cell periphery (ten cells average) was still low (and thus retained in the GA area in the cell center) at a time when in control cells VSVG-GFP had been transported to the PM (Figure 3D). Pulse antibody labeling of VSVG on the surface of PDGF treated PKD-kd-expressing cells confirmed the inhibi-

tion of anterograde transport and lack of reinternalization of VSVG after secretion (Figure 3M). Together, these results show that exogenous activation of the Rac1 pathway can induce lamellipodial activity in PKD-kd-expressing cells independent of the anterograde membrane trafficking pathway. These motile activities, however, are not limited to the leading edge as in untreated control cells, suggesting that the mechanism that normally restricts the activating signal to the leading edge is disrupted in cells where anterograde membrane traffic is inhibited.

Discussion

In this paper, our goal was to test for the requirement of the anterograde membrane transport pathway in cell locomotion and to gain insight into its possible functions in lamellipodial activity and the retrograde flow of cell surface proteins. To achieve this, we specifically inhibited TGN-to-PM membrane transport in 3T3 cells with a dominant-negative mutant of PKD1 [19]. We found that this inhibits membrane vesicle fission from the TGN and thus blocks transport of anterograde cargo to the PM. This has been previously reported for human HeLa cells [19], indicating that the role of PKD in anterograde membrane transport is well conserved. Further, we found that PKD-kd expression inhibits Swiss 3T3 fibroblast migration and greatly diminishes retrograde flow and lamellipodial activity. These effects were specific to the inhibition of PKD on the TGN, since expression of kinase-dead mutants of PKD that were unable to bind the PM and/or TGN and did not block anterograde transport also did not affect cellular motile behavior. This strongly suggests that it is the PKD-mediated blockage of TGN-to-PM vesicular transport that specifically inhibits cell motile activities and that it is not due to PKD-related functions at other cell sites such as the PM, the cytoplasm, or in the nucleus. To confirm this, we showed that inhibition of anterograde membrane transport with a GDP bound inactive ARF1-T31N mutant also inhibits cell migration. We chose PKD inhibition as our primary means of blocking secretion because it acts on a late stage in the pathway, and we wanted to inhibit the secretion pathway as close to its end as possible. Since ARF1 regulates the exit of cargo from the ER and thus acts earlier in the anterograde pathway than PKD, its inhibition may have more global consequences on intracellular trafficking due to possible divergence of the transport pathways. There is still a possibility that other unknown, nonoverlapping functions of ARF1 and PKD, inhibited in our experiments, may be independently responsible for the blockage of cell motility. PKD, for instance, could also act on substrates that transiently visit the TGN surface and, once phosphorylated, go on to have effects on motile functions at distant sites such as the leading edge. However, this is unlikely, because PM-associated PKD would most likely be expected to have direct effects on lamellipodial function, while our experiments show that it does not (Figure 4C).

What might be the essential role for anterograde membrane transport in cell motile functions? One hypothesis is that it may supply materials for retrograde surface flow and/or advancement of the lamellipodium. In support of this, we found that lamellipodial protrusion and the retrograde flow of surface bound beads was blocked by inhibition of PKD-mediated TGN to PM membrane transport. However, blocking anterograde membrane transport did not simply uncouple surface flow from the underlying actin meshwork flow, since direct imaging of fluorescent actin filaments showed that actin retrograde flow was also impaired in PKD-kd-expressing cells. It is unlikely that TGN-derived membrane vesicles destined to the leading edge PM contain actin monomers to supply actin polymerization, as vesicle contents would be exocytosed upon fusion with the PM and thus become unavailable to support filament assembly inside the cell. Alternatively, interesting candidates for structural molecules that could be delivered to the PM by anterograde transport are transmembrane integrins that mediate the adhesion of leading edge protrusions to the extracellular matrix via focal contacts. Fibroblasts are known to leave a "trail" of molecules, including integrins, on the substrate when they migrate in culture [34, 35]. Therefore, although some integrins may be recycled, as in neutrophils [36], fibroblasts must also rely on de novo synthesis and anterograde secretion to replenish integrins at the leading edge. Indeed, paxillin, another component of focal contacts, is recruited to contacts in an ARF1-dependent manner, indicating a requirement for transport through the Golgi apparatus [37]. Finally, it has been shown that a factor involved in remodeling of focal adhesions requires kinesin-dependent, MT-based transport, suggesting that it may come on anterograde membrane vesicles [38].

We also found that exogenous activation of the Rac1 pathway restored lamellipodial activity in PKD-kd-expressing cells. This activity, however, was not confined to the leading edge as in control migrating cells. Instead, it occurred around the entire cell periphery, accounting for the fact that the migration of these cells was less persistent and did not return to control levels. These results suggest that in addition to, or instead of, providing structural components required for motility, polarized TGN-to-PM trafficking is required to deliver a localized signal to regulate Rac1 activity at the leading edge. Since Rac1 is a well-characterized regulator of actin polymerization in lamellipodia [32, 33], this is likely the explanation for the inhibition of actin retrograde flow that we observed at the edges of PKD-kd-expressing cells. Alternatively, it is possible that exogenous Rac1 activation or PDGF treatment could override the dominant effect of PKD-kd. However, this is unlikely since PKD-kd was still effective at blocking TGN-to-PM transport in PDGF-treated cells (Figures 3D and 3M). We suggest that anterograde transport from the TGN to the leading edge delivers some regulatory molecule upstream of Rac1 and/or Rac1 itself. For example, it is known that H-Ras, an upstream activator of Rac1 [33, 39], is delivered to the PM by the exocytic pathway [40], and Cdc42, which is localized to GA membranes, can also activate Rac1 [32, 41]. Integrins delivered by the anterograde pathway could play both a structural and regulatory role in cell motility, as integrins can also regulate Rac1 [42]. A challenge for the future will be to distinguish between these possibilities and pinpoint the

anterograde cargo molecules needed for effective migration.

Conclusions

Our results provide the first direct evidence for the requirement of anterograde membrane trafficking pathway in cell migration. We suggest that polarized secretion delivers cargo that directs localized signaling for persistent leading edge activity necessary for directional migration.

Experimental Procedures

c-DNA Constructs

PKD mutants in pEGFP-C1 and pME-Py-GST vectors (Clontech) were obtained from Vivek Malhotra and Yusuke Maeda, UCSD [19]. pEGFP-C1 vector was used as a control for PKD-kd-GFP injections. PKD-kd-P155G/P287G-GFP and PKD-kd-P155G-GFP were created by subcloning the PKD-kd-P155G/P287G and PKD-kd-P155G fragments from the pME-GST vectors to the pEGFP-C1 vector. Temperature-sensitive folding mutant of Vesicular Stomatitis Virus G protein ts045 VSVG-GFP in pEGFP-N1 vector (Clontech) was the kind gift of Jamie White (EMBL, Heidelberg, Germany). The construct encoding myc-Rac1-Q61L in a pRK5m vector was a gift from Mira Krendel and Gary Bokoch (TSRI, La Jolla, CA).

Cell Culture, Microinjection, and Expression of Proteins

Swiss 3T3 mouse fibroblasts were cultured in DMEM supplemented with 10% fetal bovine serum (Gibco) and 2 mM L-glutamine at 37°C in humidified atmosphere of 5% CO_2. cDNA expression constructs (50–150 μg/ml in water) were microinjected in cell nuclei using an Eppendorf (Hamburg, Germany) microinjection system. Cells were allowed to express GFP-fusion constructs for at least 4 hr prior to imaging. For live cell imaging, coverslips of injected cells were mounted in double-stick tape chambers, Rose chambers, or custom-made aluminum slide chambers in phenol-free DMEM with 10 mM HEPES (pH 7.4). Individual, randomly migrating cells were used in all experiments except the first (Figure 1A), when the experimental wound assay was performed [14].

Cells injected with the VSVG-GFP construct were allowed to recover at 37°C for 30 min and then were incubated at 40°C for 4–15 hr for expression and accumulation of VSVG-GFP in the ER. For PKD-kd-GFP and myc-Rac1-Q61L coexpressing cells, anti-myc immunolabeling of the fixed cells showed that all cells examined expressing PKD-kd-GFP also expressed Rac1-Q61L.

To examine the effects of PDGF on VSVG-GFP trafficking in cells that were coexpressing PKD-kd-GST, we let the cells accumulate VSVG-GFP in the ER by incubating them at 40°C for 5 hr, shifted the cells to 37°C for 40–60 min to allow transport of VSVG-GFP to the GA/TGN, then added PDGF; 10–15 min later, we observed anterograde membrane transport from the TGN.

Myc-tagged ARF1-T31N protein (gift of Bill Balch, TSRI) was injected at ~1.2 mg/ml in buffer containing 25 mM Hepes, 125 mM potassium acetate, 1 mM magnesium acetate, and supplemented with 20 mM Alexa Fluor 568 dextran (Molecular Probes) to mark injected cells.

Live-Cell Microscopy

High-resolution time-lapse live cell imaging of GFP fusion proteins and rhodamine-labeled actin was performed on the spinning disk confocal microscope system described in [30, 43] using 60× or 100× 1.4 NA PlanApo objective lenses. Temperature was controlled using a custom-modified stage incubator (Binomic Controller BC-100, 20-20 Technologies). Images were collected at 5 or 10 s intervals. Cell motility and retrograde flow of aminated polystyrene beads [4] on the cell surface was monitored by phase contrast microscopy using either a 10× NA 0.25, a 20× NA 0.5, or a 40× NA 0.7 objective lens on an inverted microscope (Nikon TE 200) equipped with a KP-M2U video-CCD camera (Hitachi Denshi, Ltd.). We monitored the activity of multiple cells per experiment by sequential acquisition of images at multiple stage positions over time using a robotic MS-2000 XYZ microscope stage (Applied Scientific Instrumentation, Inc.) equipped with linear feedback controllers (Haidenhain) on all three axes. The temperature on the stage was controlled by an ASI 400 Air Stream Incubator (Nevtek). The microscope functions were controlled by MetaView software (Universal Imaging). Images were typically collected at 4 min intervals.

For imaging actin dynamics by fluorescent speckle microscopy, [12, 30] 4 μg/ml of rhodamine-conjugated actin were coinjected into the nucleus with the PKD-kd-GFP-encoding plasmid. Within the 4–5 hr needed for expression of the plasmid, labeled actin was exported from the nucleus and incorporated into the cytoskeleton. Images were acquired at 10 s intervals on the spinning-disk confocal microscope [43]. To prevent photobleaching of the fluorophore and oxidation damage to the cells, 0.5–1.0 U/ml of oxyrase (Oxyrase, Inc.) was added to the filming media.

Immunocytochemistry

Coverslips of cells were briefly rinsed in PBS (0.9% NaCl, 10 mM sodium phosphate [pH 7.2]) and then fixed in −20°C methanol for 5 min. Alternatively, to preserve the fragile PKD-kd-induced membrane tubules, they were prefixed in 0.25% glutarladehyde in BRB80 buffer (80 mM PIPES, 1 mM $MgCl_2$, 1 mM EGTA [pH 6.8] with KOH) for 30 s, then fixed and lysed in 0.25% glutaraldehyde plus 0.1% triton X-100 in BRB80 for 10 min, rinsed, and quenched with freshly prepared 0.2% sodium borohydrate in PBS. Nuclei were visualized with DAPI. Actin was visualized with x-rhodamine-conjugated phalloidin (Molecular Probes). Microtubules were immunolabeled with monoclonal DM1A (Sigma), medial GA with anti-mannosidase-II polyclonal antibodies (gift from Bill Balch, TSRI), TGN with anti-TGN38 antibodies (Accurate Chemical & Scientific Corporation). Mouse Mab1I antibodies against the extracellular domain of VSVG were a generous gift from M. Perez and M. Oldstone (TSRI). All fluorescent secondary antibodies were obtained from Jackson ImmunoResearch.

Image Processing and Data Analysis

Micrographs were calibrated using images of a stage micrometer. All measurements were performed in MetaMorph and the data transferred to Excel (Microsoft, Inc.) for analysis.

Image features of interest were tracked in serial images using the track object function in Metamorph. Locomotory activity of cells was determined from the instantaneous velocities of the cell nucleus at 4 min intervals. Statistical samples were formed by breaking the 4 min interval measurements into groups of five (i.e., 20 min). The average over each group constituted one data point. The standard error of the mean is given by the standard deviation divided by the square root of the total number of 20 min intervals. The same method was used to calculate velocity of VSVG-GFP-containing cargo carriers and the tips of PKD-kd-induced membrane tubules except that 10 s intervals and 1 min groups were used.

To quantify the rate of VSVG-GFP transport through the secretory pathway, we measured the ratio of peripheral to total cell fluorescence over time. The peripheral fluorescence was estimated by averaging the fluorescence of three small regions at the cell periphery, next to the cell edge (5% of total area each). When VSVG-GFP was localized in the ER (which extends throughout the cell), the GA (which is in the cell center), or the PM (which surrounds the entire cell), the relative peripheral fluorescence was high, low, or high, respectively. Thus, measuring this ratio over time after shifting to the permissive temperature (37°C) for synchronous release of VSVG-GFP from the ER reflected VSVG-GFP transport through the secretory pathway. Note that the earliest time point when we could record images (labeled as "time 0") was within 1–2 min after temperature shift. Relative fluorescence intensity of the anti-VSVG antibody labeling of the bottom surface of the cell was measured from maximal projection of two immunofluorescence confocal sections and then normalized to the total amount of cellular VSVG-GFP fluorescence measured from maximal projections of several confocal sections spanning the whole thickness of the cell.

Supplemental Data

Supplemental Data including QuickTime movies to supplement the figures are available at http://www.current-biology.com/cgi/content/full/14/2/88/DC1/.

Acknowledgments

We thank Vivek Malhotra and Yusuke Maeda (UCSD) for their support, insightful discussions and PKD constructs; Bill Balch (TSRI) for anti-mannosidase II antibodies and ARF1 protein; M. Perez and M. Oldstone (TSRI) for anti-VSVG antibodies, and members of the Waterman lab, Sandy Schmid and Hanna Damke (TSRI) for helpful discussions. N.P. is supported by Leukemia and Lymphoma Society Career Development grant # 5195-03. Supported by NIH GM-61804-03 to CMWS.

Received: June 30, 2003
Revised: October 10, 2003
Accepted: November 20, 2003
Published: January 20, 2004

References

1. Elson, E.L., Felder, S.F., Jay, P.Y., Kolodney, M.S., and Pasternak, C. (1999). Forces in cell locomotion. Biochem. Soc. Symp. *65*, 299–314.
2. Heath, J.P., and Holifield, B.F. (1991). Cell locomotion: new research tests old ideas on membrane and cytoskeletal flow. Cell Motil. Cytoskeleton *18*, 245–257.
3. Mitchison, T.J., and Cramer, L.P. (1996). Actin-based cell motility and cell locomotion. Cell *84*, 371–379.
4. Lin, C.H., and Forscher, P. (1995). Growth cone advance is inversely proportional to retrograde F-actin flow. Neuron *14*, 763–771.
5. Abercrombie, M., Heaysman, J.E., and Pegrum, S.M. (1970). The locomotion of fibroblasts in culture. 3. Movements of particles on the dorsal surface of the leading lamella. Exp. Cell Res. *62*, 389–398.
6. Dembo, M., and Harris, A.K. (1981). Motion of particles adhering to the leading lamella of crawling cells. J. Cell Biol. *91*, 528–536.
7. Bretscher, M.S. (1976). Directed lipid flow in cell membranes. Nature *260*, 21–23.
8. Kucik, D.F., Elson, E.L., and Sheetz, M.P. (1990). Cell migration does not produce membrane flow. J. Cell Biol. *111*, 1617–1622.
9. Sheetz, M.P., Turney, S., Qian, H., and Elson, E.L. (1989). Nanometre-level analysis demonstrates that lipid flow does not drive membrane glycoprotein movements. Nature *340*, 284–288.
10. Lee, J., Gustafsson, M., Magnusson, K.E., and Jacobson, K. (1990). The direction of membrane lipid flow in locomoting polymorphonuclear leukocytes. Science *247*, 1229–1233.
11. Wang, Y.L. (1985). Exchange of actin subunits at the leading edge of living fibroblasts: possible role of treadmilling. J. Cell Biol. *101*, 597–602.
12. Waterman-Storer, C.M., Desai, A., Bulinski, J.C., and Salmon, E.D. (1998). Fluorescent speckle microscopy, a method to visualize the dynamics of protein assemblies in living cells. Curr. Biol. *8*, 1227–1230.
13. Etienne, M., and Hall, A. (2001). Integrin-mediated activation of Cdc42 controls cell polarity in migrating astrocytes through PKCzeta. Cell *106*, 489–498.
14. Kupfer, A., Louvard, D., and Singer, S.J. (1982). Polarization of the Golgi apparatus and the microtubule-organizing center in cultured fibroblasts at the edge of an experimental wound. Proc. Natl. Acad. Sci. USA *79*, 2603–2607.
15. Bergmann, J.E., Kupfer, A., and Singer, S.J. (1983). Membrane insertion at the leading edge of motile fibroblasts. Proc. Natl. Acad. Sci. USA *80*, 1367–1371.
16. Kupfer, A., Kronebusch, P.J., Rose, J.K., and Singer, S.J. (1987). A critical role for the polarization of membrane recycling in cell motility. Cell Motil. Cytoskeleton *8*, 182–189.
17. Bershadsky, A.D., and Futerman, A.H. (1994). Disruption of the Golgi apparatus by brefeldin A blocks cell polarization and inhibits directed cell migration. Proc. Natl. Acad. Sci. USA *91*, 5686–5689.
18. Valverde, A.M., Sinnett-Smith, J., Van Lint, J., and Rozengurt, E. (1994). Molecular cloning and characterization of protein kinase D: a target for diacylglycerol and phorbol esters with a distinctive catalytic domain. Proc. Natl. Acad. Sci. USA *91*, 8572–8576.
19. Liljedahl, M., Maeda, Y., Colanzi, A., Ayala, I., Van Lint, J., and Malhotra, V. (2001). Protein kinase D regulates the fission of cell surface destined transport carriers from the trans-Golgi network. Cell *104*, 409–420.
20. Prestle, J., Pfizenmaier, K., Brenner, J., and Johannes, F.J. (1996). Protein kinase C mu is located at the Golgi compartment. J. Cell Biol. *134*, 1401–1410.
21. Rey, O., and Rozengurt, E. (2001). Protein kinase D interacts with Golgi via its cysteine-rich domain. Biochem. Biophys. Res. Commun. *287*, 21–26.
22. Baron, C.L., and Malhotra, V. (2001). Role of diacylglycerol in PKD recruitment to the TGN and protein transport to the plasma membrane. Science *295*, 325–328.
23. Maeda, Y., Beznoussenko, G.V., Van Lint, J., Mironov, A.A., and Malhotra, V. (2001). Recruitment of protein kinase D to the trans-Golgi network via the first cysteine-rich domain. EMBO J. *20*, 5982–5990.
24. Matthews, S.A., Iglesias, T., Rozengurt, E., and Cantrell, D. (2000). Spatial and temporal regulation of protein kinase D (PKD). EMBO J. *19*, 2935–2945.
25. Matthews, S., Iglesias, T., Cantrell, D., and Rozengurt, E. (1999). Dynamic re-distribution of protein kinase D (PKD) as revealed by a GFP-PKD fusion protein: dissociation from PKD activation. FEBS Lett. *457*, 515–521.
26. Van Lint, J., Rykx, A., Maeda, Y., Vantus, T., Sturany, S., Malhotra, V., and Vandenheede, J.R. (2002). Protein kinase D: an intracellular traffic regulator on the move. Trends Cell Biol. *12*, 193–200.
27. Bankaitis, V.A. (2002). Cell biology. Slick recruitment to the Golgi. Science *295*, 290–291.
28. Hirschberg, K., Miller, C.M., Ellenberg, J., Presley, J.F., Siggia, E.D., Phair, R.D., and Lippincott-Schwartz, J. (1998). Kinetic analysis of secretory protein traffic and characterization of golgi to plasma membrane transport intermediates in living cells. J. Cell Biol. *143*, 1485–1503.
29. Dascher, C., and Balch, W.E. (1994). Dominant inhibitory mutants of ARF1 block endoplasmic reticulum to Golgi transport and trigger disassembly of the Golgi apparatus. J. Biol. Chem. *269*, 1437–1448.
30. Salmon, W.C., Adams, M.C., and Waterman-Storer, C.M. (2002). Dual-wavelength fluorescent speckle microscopy reveals coupling of microtubule and actin movements in migrating cells. J. Cell Biol. *158*, 31–37.
31. Wittmann, T., Bokoch, G.M., and Waterman-Storer, C.M. (2003). Regulation of leading edge microtubule and actin dynamics downstream of Rac1. J. Cell Biol. *161*, 845–851.
32. Ridley, A.J., Paterson, H.F., Johnston, C.L., Diekmann, D., and Hall, A. (1992). The small GTP-binding protein rac regulates growth factor-induced membrane ruffling. Cell *70*, 401–410.
33. Ridley, A.J. (2001). Rho GTPases and cell migration. J. Cell Sci. *114*, 2713–2722.
34. Palecek, S.P., Schmidt, C.E., Lauffenburger, D.A., and Horwitz, A.F. (1996). Integrin dynamics on the tail region of migrating fibroblasts. J. Cell Sci. *109*, 941–952.
35. Chen, W.T. (1981). Mechanism of retraction of the trailing edge during fibroblast movement. J. Cell Biol. *90*, 187–200.
36. Lawson, M.A., and Maxfield, F.R. (1995). Ca(2+)- and calcineurin-dependent recycling of an integrin to the front of migrating neutrophils. Nature *377*, 75–79.
37. Norman, J.C., Jones, D., Barry, S.T., Holt, M.R., Cockcroft, S., and Critchley, D.R. (1998). ARF1 mediates paxillin recruitment to focal adhesions and potentiates Rho-stimulated stress fiber formation in intact and permeabilized Swiss 3T3 fibroblasts. J. Cell Biol. *143*, 1981–1995.
38. Kaverina, I.N., Minin, A.A., Gyoeva, F.K., and Vasiliev, J.M. (1997). Kinesin-associated transport is involved in the regulation of cell adhesion. Cell Biol. Int. *21*, 229–236.
39. Lambert, J.M., Lambert, Q.T., Reuther, G.W., Malliri, A., Siderovski, D.P., Sondek, J., Collard, J.G., and Der, C.J. (2002). Tiam1 mediates Ras activation of Rac by a PI(3)K-independent mechanism. Nat. Cell Biol. *4*, 621–625.
40. Apolloni, A., Prior, I.A., Lindsay, M., Parton, R.G., and Hancock,

J.F. (2000). H-ras but not K-ras traffics to the plasma membrane through the exocytic pathway. Mol. Cell. Biol. *20*, 2475–2487.

41. Erickson, J.W., Zhang, C., Kahn, R.A., Evans, T., and Cerione, R.A. (1996). Mammalian Cdc42 is a brefeldin A-sensitive component of the Golgi apparatus. J. Biol. Chem. *271*, 26850–26854.
42. Price, L.S., Leng, J., Schwartz, M.A., and Bokoch, G.M. (1998). Activation of Rac and Cdc42 by integrins mediates cell spreading. Mol. Biol. Cell *9*, 1863–1871.
43. Adams, M.C., Salmon, W.C., Gupton, S.L., Cohan, C.S., Wittmann, T., Prigozhina, N., and Waterman-Storer, C.M. (2003). A high-speed multi-spectral spinning disk confocal microscope system for fluorescent speckle microscopy of living cells. Methods *1*, 29–41.